PHYSICAL REVIEW E **71**, 065701(R) (2005)

Phase behavior of a three-dimensional core-softened model system

D Quigley* and M. I. J. Probert
University of York, Heslington, York YO10 5DD, United Kingdom
(Received 25 November 2004; published 21 June 2005)

The phase behavior of a three-dimensional model substance interacting via a continuous core-softened pair potential is studied. A combination of thermodynamic integration and free-energy augmented metadynamics is employed to identify the ground state structure as simple hexagonal. A transition to close packing is predicted at high pressure. The melting line is traced, which when combined with the liquid-vapor line, allows the liquid to be studied over its entire thermodynamically stable range. We find no liquid anomalies in the range of pressures for which the vaporization transition exists. Our results therefore support suggestions that the anomalous behavior of such fluids is unique to the two-dimensional case.

DOI: 10.1103/PhysRevE.71.065701 PACS number(s): 61.20.Ja, 61.66.Bi, 64.70.Dv, 64.70.Fx

I. INTRODUCTION

Interest in fluids interacting via core-softened pair potentials originates in the work of Stell and Hemmer [1]. They proposed that such models may lead to a liquid-liquid phase transition and an associated second critical point. Recently, the experimental observation of a first-order liquid-liquid transition in high pressure phosphorus [2] has created new interest in understanding these models and their possible application to liquid metals.

Recently, Wilding and Magee [3] have categorized the various forms of core-softened potential as either "ramp" or "shoulder" potentials. Ramp potentials are purely repulsive and have been shown to lead to a stable liquid-liquid transition [3,4] in both two and three dimensions. Shoulder potentials include an attractive component and have been studied in two forms. The first is discontinuous, constructed as an attractive well and a repulsive inner step (Fig. 1). The second is continuous, constructed as a superposition of the familiar Lennard-Jones potential and a second Gaussian minimum (Fig. 1).

$$\Phi(\mathbf{r}^N) = \sum_{j>i}^{N} 4\epsilon\left[\left(\frac{\sigma}{r_{ij}}\right)^{12} - \left(\frac{\sigma}{r_{ij}}\right)^{6}\right] - A\exp[-w(r_{ij}-r_0)^2]. \tag{1}$$

The phase behavior of the shoulder model in two dimensions has been the subject of considerable study. Liquid-state anomalies similar to those observed in water have been reported, and related to a possible metastable liquid-liquid critical point [5,6]. Other work suggests that the anomalies are an early manifestation of the freezing transition, in which solid clusters form with lower density than the surrounding liquid [3].

Extensive studies of the shoulder potential in three dimensions have been restricted to the discrete form [7–9]. For certain parametrizations, these manifest two liquid phases, with no liquid anomalies and a single solid phase. The 3D smooth shoulder potential has been the subject of two limited studies. The first [10] explored only the high temperature liquid, well above the melting line. Unsurprisingly, no liquid anomalies were found. The second study [11] has measured a diffusion anomaly at somewhat lower temperatures. Simulations were conducted over a metastable density range for which the pressure is negative with the potential used. No simulation has yet explored the low temperature liquid in a thermodynamically stable state, or located the melting line and the associated solid structure.

We address this omission with a complete mapping of the phase diagram, up to the critical pressure, for a 3D smooth shoulder potential. We then search the stable liquid for anomalies. In this Rapid Communication, we report on the potential in Fig. 1 for which $A=\epsilon$. We find this to be the first such potential on increasing the parameter A for which the structure of the solid at the melting line is no longer close packed. Detailed studies of potentials with other positive A parameters will be reported at a later date. We do not vary the parameters w and r_0 in the work reported here. The potential is truncated at $r_{ij}=2.5\sigma$ and shifted such that force varies continuously to zero at the cutoff.

Measured quantities are presented here in the usual dimensionless reduced units. Energies are quoted as multiples of the inner-well depth ϵ, lengths as multiples of σ. Reduced temperature T^* is calculated as k_BT/ϵ, with pressure $P^*=P\sigma^3/\epsilon$. Time is measured in units $t^*=(m/\epsilon)^{1/2}\sigma$ where m is the atomic mass. In all dynamical simulations a time-step $\Delta t^*=0.001$ is used. Important parameters for our simulations

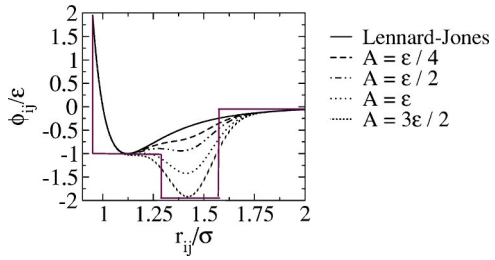

FIG. 1. Smooth "shoulder" pair potential defined in Eq. (1) compared to the Lennard-Jones potential and an equivalent discontinuous potential. Parameters are $r_0=1.43\sigma$ and $w=41.22\sigma^{-2}$. All quantities plotted are dimensionless.

*Electronic address: dq100@york.ac.uk

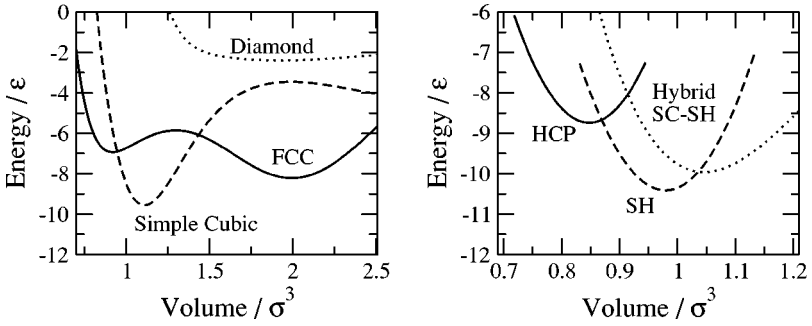

FIG. 2. Energy per atom vs reduced volume for a selection of simple isotropic structures (left) and for anisotropic structures identified by the metadynamics or otherwise (right). All quantities plotted are dimensionless.

are presented here. Further details of our simulations will be reported in a later Communication.

II. SOLID PHASES

To identify the solid phase structure, energy-volume curves were traced for a variety of isotropic structures as shown in Fig. 2. The fcc structure appears metastable at two different densities. This has been confirmed to be the case at $T^*=0.167$, $P^*=0.024$ via constant pressure Langevin dynamics simulations within a fully flexible cell. The peak in the pair correlation function corresponding to the Lennard-Jones minimum is absent in the lower density structure, the nearest-neighbor distance being r_0.

The lowest energy in this subset of possible structures is that of simple cubic (sc) symmetry. Beginning from this configuration, a metadynamics exploration of the free-energy surface is implemented, as described by Martoňák, Laio, and Parrinello in Ref. [12], and briefly summarized below.

In the initial configuration, *NVT* Langevin dynamics simulations (canonical ensemble) are performed in a fixed cell with periodic boundary conditions. After an equilibration period of 1000 steps, the pressure tensor is averaged over a further 2000, and used to compute the derivative of the Gibbs free energy with respect to the vector **h**, which contains the six independent components of the symmetrized matrix of cell vectors. A steepest descent step of length δh is then taken in **h**, during which the fractional coordinates of the atoms themselves are held constant. This constitutes one metadynamics step.

At subsequent steps, the steepest descent force $\mathbf{F}_{\mathrm{sd}}$ is supplemented by a history dependent force $\mathbf{F}_{\mathrm{aug}}$ representing the effect of augmenting the free energy surface with a Gaussian of height W at every point **h** already visited by the metadynamics. The long term effect of these augmentations is to drive the system away from the initial basin of attraction and into a second, corresponding to a new crystal structure.

Our metadynamics are conducted at a temperature $T^*=0.25$ and pressure $P^*=0.023$. This state point is expected to lie well below the melting temperature. The *NVT* Langevin dynamics simulations employ a friction coefficient $\gamma^*=2.3$ and are conducted using the method described in Sec. II of Ref. [13].

The lowest energy structure was generated from a run of 100 metasteps as shown in Fig. 3. A step δh of 1.16σ is used, with free-energy augmentations 2.63ϵ in height. The final configuration is then optimized using damped dynamics of both the atomic and cell degrees of freedom. The result is easily identified as a $5\times5\times5$ repetition of a simple hexagonal (sh) primitive cell ($\alpha=\beta=90°, \gamma=120°$) with $a=b=1.059\sigma$ and $c=1.016\sigma$.

A number of hybrid structures in which stacking alternates between sc and sh have also been located when employing smaller δh. Energy vs volume curves for the sh, hcp, and lowest energy sc-sh hybrid are also plotted in Fig. 2 by optimizing anisotropically to a series of specified hydrostatic pressures. A common tangent construction reveals the zero temperature sh-hcp transition occurs at $P^*=12.90$.

Free-energy calculations for these structures have been performed using the Einstein crystal method of Frenkel and Ladd [14]. An optimal zero pressure cell for the thermodynamic integration is first identified at various temperatures by averaging over a 100,000 Δt constant pressure (NPT) Langevin dynamics [13] trajectory. These employ a relaxation time for the simulation cell of $t^*_{\mathrm{cell}}=70.0$. Fifty points are sampled along the path connecting the core-softened crystal to the reference system. At each point *NVT* Langevin dynamics simulations are performed employing the required center of mass constraint, equilibrating for 1000 steps and sampling the free-energy derivative for a further 3000. A particle friction coefficient of $\gamma^*=2.3$ is used in both the *NVT* and NPT simulations. The resulting free energies are shown in Fig. 4, indicating that the sh structure will be favored over the temperature range shown.

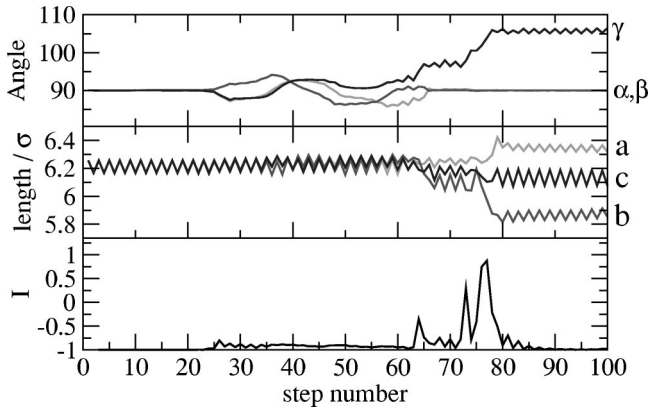

FIG. 3. Evolution of the cell angles (in degrees) and cell lengths (in units of the Lennard-Jones length parameter σ) during a metadynamics run initialized from the simple cubic minimum. The dimensionless quantity $I=\mathbf{F}_{\mathrm{sd}}\cdot\mathbf{F}_{\mathrm{aug}}/|\mathbf{F}_{\mathrm{sd}}||\mathbf{F}_{\mathrm{aug}}|$ is expected to remain at ≈-1 while exploring the initial basin of attraction, and peak sharply at +1 at the cusp between two minima.

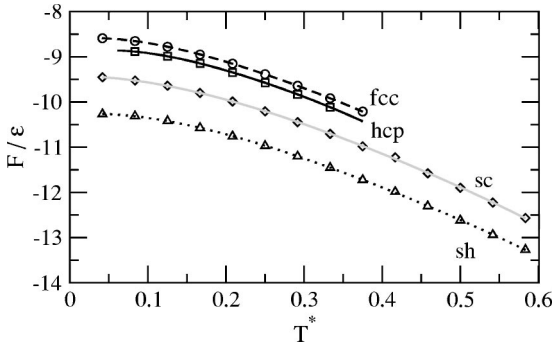

FIG. 4. Free energy in multiples of ϵ per atom vs reduced temperature $T^*=k_BT/\epsilon$, for the lowest energy candidate structures at zero pressure. Both quantities are dimensionless. The sh structure remains favorable over this temperature range.

III. MELTING CURVE

An initial point on the melting curve is first measured using molecular dynamics simulations of enforced coexistence, a method similar to that in Ref. [15]. A supercell of the sh structure containing 864 atoms is prepared, one half of which is heated to beyond the point of mechanical instability at $T^*=1.5\epsilon$ while constraining the remaining half. The resulting configuration is then simulated at a specified pressure using a psuedo-NPH (isobaric-isoenthalpic ensemble) ensemble, employing the fully-flexible NPT equations of Ref. [16] with the Nosé-Hoover chains removed. In this ensemble the conserved quantity is $H+K_{\mathrm{cell}}$ (enthalpy plus fictitious kinetic energy of the cell). The NPH ensemble is therefore not reproduced exactly due to fluctuations in K_{cell}.

Despite this, provided that care is taken in ensuring these fluctuations are very much less than the latent heat of formation per atom, the system remains in a equally mixed state. The resulting average temperature (sampled over 100 000 time steps) at equilibrium is therefore that of the melting transition. With a conserved quantity of 8.2ϵ/atom, and a volume relaxtion time of $t^*_{\mathrm{cell}}=70.0$, the rms. fluctuation in enthalpy is less than 0.05ϵ/atom at a pressure of $P^*=0.238$. This compares to a latent heat of 2.16ϵ/atom. The corresponding average temperature in this simulation was measured to be $T^*=0.609$.

This point is then used to initiate a Gibbs-Duhem integration series [17], tracing the melting curve in the direction of decreasing temperature. At each integration step, the slope of the melting curve is calculated from a *NPT* Langevin dynamics simulation of each phase. Equilibration is performed over 5000 time steps, before sampling for a further 10 000. 392 atoms are simulated in the solid phase, and 256 in the liquid. A small integration step in inverse temperature ensures accuracy of integration, resulting in 60 calculated points on the melting curve as shown in Fig. 5. The final point of the series is confirmed to lie on the melting curve with a second coexisting simulation.

Combined with the expected sh-hcp transition pressure, and the free-energy calculations in the previous section, it is clear that the sh structure will be the favored solid over the pressure range of interest here.

IV. LIQUID-VAPOR TRANSITION

To trace the liquid vapor curve and locate the critical point, the now standard combination of histogram reweighting and multicanonical sampling is employed. This scheme is based on Monte-Carlo simulation in the grand-canonical ensemble. See, e.g., Ref. [18] for details. Simulations are performed in a cube of side 7.13σ over 600 000 attempted particle insertions/removals. The coexistence curve is traced in steps of $\Delta T^*=0.008$ down to a temperature of $T^*=1.5$. Below this temperature the large density difference between the two phases makes multicanonical sampling expensive. The critical temperature is estimated by extrapolating the density difference $\Delta\rho$ to zero using the expected $\Delta\rho\propto(T-T_c)^{\beta}$ relationship with the exponent β as a fitting parameter. The resulting value (uncorrected for finite size effects) is $T^*=1.683$, and occurs at a pressure of $P^*=0.142$.

For temperatures below $T^*=1.5$, Gibbs-Duhem integration is used to trace the remainder of the coexistence curve. This is initiated from a point in the P-T plane obtained via a numerical fit to thermodynamic data, as unfolded from the multicanonical simulations. A system of 256 atoms is used for both phases equilibrating for 10 000 time steps before sampling the enthalpy and volume for a further 50 000 steps. A small step in inverse temperature ensures accuracy of integration, resulting in 115 sampled points on the curve between $T^*=1.5$ and the melting temperature.

V. LIQUID

With the full range of temperatures over which the liquid is stable now identified, the search for liquid state anomalies can proceed. Particular effort is spent close to the melting

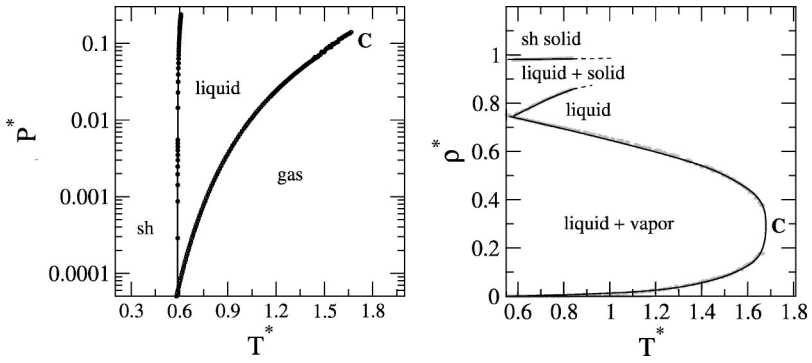

FIG. 5. Phase diagram of the potential studied in this work. The reduced units are $T^*=k_BT/\epsilon$, $P^*=\sigma^3P/\epsilon$, $\rho^*=\rho\sigma^3$. Each is dimensionless. Pressure is plotted on a logarithmic (base 10) scale. The approximate liquid-gas critical point located as described in Sec. IV is labeled C. The sh-hcp transition lies well above the pressure range studied here.

line, sampling at a smaller temperature interval in this region. Specifically NPT molecular dynamics simulations are conducted at temperatures from $T^*=0.625$ to 0.708 in steps of 0.008, from 0.708 to 0.833 in steps of 0.042, and then up to the liquid-vapor transition in steps of 0.167. Each simulation consists of 500 000 steps at equilibrium, using 500 atoms in a cubic cell. Anomalies are sought along two isobars, at pressure of $P^*=0.047$ and 0.118.

By plotting the average internal energy and cell dimension as a function of temperature, it is possible to identify any anomalies in the constant pressure heat capacity C_p, and the isobaric expansivity α_p. Isothermal modulus β_T is computed from the equilibrium fluctuations in volume, and the diffusion coefficient D is calculated from the gradient of the mean-square atomic displacement.

The results show, that to within the error imposed by the finite system size and simulation time, no anomalies are apparent in any of these quantities within the stable liquid regime. No evidence of a second liquid phase is detected, negating the need for further multicanonical or Gibbs ensemble [19] simulations.

VI. CONCLUSIONS

By employing augmented metadynamics simulations combined with careful thermodynamic integration, we have shown that the solid structure of a particular core-softened potential is simple hexagonal over the entire temperature range at low pressure. A transition to a hexagonal close-packed structure is predicted at high pressure.

We have then traced the melting curve and the liquid-vapor transition, allowing study of the liquid over its entire stable temperature range. Particular attention has been paid to the region close to the freezing transition. We have found no anomalies in bulk modulus, heat capacity or thermal expansivity at constant pressure within the stable liquid. We also measure no anomaly in the diffusion coefficient. Our results suggest the anomalous behavior of core-softened fluids is limited to two dimensions. We note that in Ref. [9] two liquid phases were only observed for potentials in which the inner shoulder is of positive energy with respect to the long range tail. This property cannot be reproduced with a Lennard-Jones plus Gaussian superposition as we have employed here, a fundamental difference between the smooth and discrete versions.

We have not explored the liquid in the high pressure regime close to the expected sh-hcp transition in the solid, and therefore cannot rule out the possible presence of liquid anomalies in this region.

ACKNOWLEDGMENTS

Computational facilities for this research were provided under EPSRC Grant No. R47769.

[1] P. Hemmer and G. Stell, Phys. Rev. Lett. **24**, 1284 (1970).
[2] Y. Katayama, T. Mizutani, W. Utsumi, O. Shimomura, M. Yamakata, and K. Funakoshi, Nature (London) **403**, 170 (2000).
[3] N. B. Wilding and J. E. Magee, Phys. Rev. E **66**, 031509 (2002).
[4] E. A. Jagla, Phys. Rev. E **63**, 061501 (2001).
[5] A. Scala, M. R. Sadr-Lahijany, N. Giovambattista, S. V. Buldyrev, and H. E. Stanley, Phys. Rev. E **63**, 041202 (2001).
[6] M. R. Sadr-Lahijany, A. Scala, S. V. Buldyrev, and H. E. Stanley, Phys. Rev. Lett. **81**, 4895 (1998).
[7] G. Franzese, G. Malescio, A. Skibinsky, S. V. Buldyrev, and H. E. Stanley, Phys. Rev. E **66**, 051206 (2002).
[8] G. Franzese, G. Malescio, A. Skibinsky, S. V. Buldyrev, and H. E. Stanley, Nature (London) **409**, 692 (2001).
[9] A. Skibinsky, S. V. Buldyrev, G. Franzese, G. Malescio, and H. E. Stanley, Phys. Rev. E **69**, 061206 (2004).
[10] P. Mausbach and H. O. May, Fluid Phase Equilib. **214**, 1 (2003).
[11] P. Netz, J. Raymundi, A. Camera, and M. Barbosa, Physica A **342**, 48 (2003).
[12] R. Martoňák, A. Laio, and M. Parrinello, Phys. Rev. Lett. **90**, 075503 (2003).
[13] D. Quigley and M. I. J. Probert, J. Chem. Phys. **120**, 11432 (2004).
[14] D. Frenkel and A. J. C. Ladd, J. Chem. Phys. **81**, 3188 (1984).
[15] D. Alfè, Phys. Rev. B **68**, 064423 (2003).
[16] G. J. Martyna, J. T. Tobias, and M. L. Klein, J. Chem. Phys. **101**, 4177 (1994).
[17] D. Kofke, J. Chem. Phys. **98**, 4149 (1993).
[18] N. B. Wilding, Am. J. Phys. **69**, 1147 (2001).
[19] A. Z. Panagiotopoulos, Mol. Phys. **61**, 813 (1987).